Effect of the oxidization of Si_3N_4 powder on the microstructural and mechanical properties of hot isostatic pressed silicon nitride

Awais Qadir[a,b]; Zsolt Fogarassy[b]; Zsolt E. Horváth[b]; Katalin Balazsi[b*]; Csaba Balazsi[b]

[a] Doctoral School on Materials Sciences and Technologies, Obuda University, Bécsi str. 96/b, 1034 Budapest, Hungary

[b] Thin Film Physics Department, Institute of Technical Physics and Materials Science, Centre for Energy Research, Hungarian Academy of Sciences, Konkoly-Thege M. str. 29-33, Budapest, Hungary

*Corresponding Author: Dr. Katalin Balazsi, balazsi.katalin@energia.mta.hu, Tel: +36 1 392 2249

Abstract

The effect of nanosized oxidized silicon nitride powder particles on the microstructural and mechanical properties of hot isostatic pressed silicon nitride was studied. The starting <alpha> Si_3N_4 powders were oxidized for 10 and 20 h at 1000 ˚C in ambient air environment. An amorphous oxide layer was observed on the surface of Si_3N_4 powder particles using high resolution transmission electron microscopy (HRTEM) whose thickness increased with the oxidation time. The powders were hot isostatic pressed at 1500 ˚C and 1700 ˚C in nitrogen gas environment under 20 Mpa for 3h. Complete <alpha> to <beta> transformation was observed in Si_3N_4 samples sintered at 1700 C under 20 MPa for 3 h compared to Si_3N_4 samples sintered at 1500 ˚C. Silicon oxynitride (Si_2N_2O) was found in sintered samples whose amount increased with the oxidation time. The <beta> phase decreased with the increase of Si_2N_2O phase in the sintered samples. The flexural strength of samples sintered at 1700 ˚C is higher due to the higher amount of <beta>-Si_3N_4 phase than for samples sintered at 1500 ˚C. Decreasing flexural strength was observed with the oxidation time. Higher amount of oxygen in the base powders resulted in a higher Si_2N_2O content in the sintered Si_3N_4.

Keywords: Silicon nitride; Oxidation; Mechanical properties; Hot isostatic pressing, Silicon Oxynitride

1. Introduction

Silicon nitride (Si_3N_4) is a high-grade structural ceramic material due to its excellent flexural strength, fracture resistance, high hardness, resistance to oxidation, thermal properties at room and elevated temperatures [1- 6]. Si_3N_4 have been applied in high speed cutting tools, bearing and sealing, gas turbine engines and different components in the aircraft's auxiliary power units [1- 6]. Two crystallographic structures of Si_3N_4 as <alpha> and <beta> has its own intrinsic properties [4, 7, 8]. The <alpha> → <beta> phase transformation occurs at high

temperature when <alpha> grains dissolve into a liquid phase and precipitate as <beta> phase [9]. More stable <beta> Si_3N_4 named as self-reinforced Si_3N_4 is characterized by elongated rod-like structure which acts as reinforcing phase in a matrix and enhance the strength of the material [10 - 12].

Si_3N_4 based materials are used in a high-temperature oxidizing environment. The knowledge of oxidation´s effect on the structural, mechanical and tribological properties is indispensable. Several scientific works have studied this effect and found that the formation of oxide layer caused the degradation of material due which resulted the lower value of mechanical properties [13 - 18]. Balazsi et al. showed the role and the effect of excess oxygen in the <alpha> - Si_3N_4 starting powder performed at 1000 °C in air for 150 h The oxidized samples was sintered by Hot isostatic pressing (HIP) at 1700 °C in high purity nitrogen at a low gas pressure of 20 bar for 1 h. They confirmed the presence of <beta> - Si_3N_4 and Si_2N_2O phases in sintered samples and glassy phases appeared after sintering [19]. The base silicon nitride powder characteristics have a significant influence on the final properties of densified product. On the other hand, the surface modifications of starting powder influenced the microstructural and mechanical properties of the densified material as well. Lot of works studied the kinetics and structural changes of surface-oxidized ~~in~~ Si_3N_4 phase [20 - 22]. Rivière et al. obtained the SiO_xN_y,-as intermediate surface composition between Si_3N_4 and silica [23]. The effect of oxidized silicon nitride starting powder on the mechanical properties of sintered material is still ambiguous. Behaviour of oxidized particles during the sintering process at different sintering temperatures is not studied yet.

The aim of this work is to study the effect of oxidized nanosized <alpha> -Si_3N_4 powder and sintering temperatures on the microstructural and mechanical properties of the hot isostatic pressed ceramics. Scanning electron microscopy (SEM), high-resolution transmission electron microscopy (HRTEM) and X-ray diffraction measurements were carried-out to characterize the powders and sintered samples. 3 and 4 points bending strength, Young's modulus, Vicker's hardness and toughness of sintered samples were measured.

2. Experimental details

2.1. Preparation of samples

The <alpha> -Si_3N_4 powder was oxidized at 1000 ˚C for 10 hours and 20 hours in ambient air, respectively. The starting powders used in experiments were as follows: 90 wt. % <alpha> Si_3N_4 powders (Unoxidized and 10 & 20 hrs oxidized <alpha> Si_3N_4 powders) (Ube, SN-ESP), as well 4 wt. % Al_2O_3 (Alcoa, A16) and 6 wt. % Y_2O_3 (H.C. Starck, grade C) sintering additives. Polyethylene glycol (PEG) surfactants and ethanol were added to the powder mixture. These mixtures were milled in high efficient attritor mill (Union Process, type 01-HD/HDDM) equipped with zirconia agitator delta discs and zirconia grinding media (diameter of 1 mm) in a 750 cm^3 zirconia tank with high rotation speed 4000 rpm for 4 hours.. Each batch contains zirconia as contamination which originated from media and discs. The details of sample composition can be seen in Table 1.

The powders were dried and sieved through 150 µm mesh number. Green samples were produced by dry pressing under 200 MPa pressure. These samples were subjected to ~~the~~ oxidation at 400 ˚C for the elimination of polyethyleneglycol (PEG) prior to the sintering process. The same powder preparation process was adopted as in Balazsi et. al publications [24].

For analysis of the effect of sintering temperature on the microstructural and mechanical properties of composites, two hot isostatic pressing sintering temperatures were carefully chosen.

a) First batch of samples was densified at 1700 °C, under 20 MPa in nitrogen (N_2) gas environment for 3 hours as a holding time.
b) Second batch of samples was densified at 1500 ˚C, under 20 MPa in nitrogen (N_2) gas environment for 3 hours as a holding time.

The heating rate did not exceed 25 ˚C/ min. The dimensions of the as-sintered specimens were 3.5 mm x 5 mm x 50 mm [19].

2.2 Characterization of Materials

Phase compositions of powders and sintered samples were analysed by X-ray diffractometer (Bruker AXS D8) with Cu Kα radiation. Morphology, shape and homogeneity of powder particles were examined by scanning electron microscopy (SEM, LEO 1540 XB). Energy Dispersive X-ray Spectroscopy (EDS) was carried out for the qualitative analysis of base powders (oxidized & unoxidized Si_3N_4 powders) for the quantification of elemental compositions. Transmission Electron Microscopy (TEM, Philips CM-20) with accelerating voltage 200 kV was carried out for the microstructural characterization of base powders. High Resolution Transmission Electron Microscopy (HRTEM, JEOL3010) with accelerating voltage 300 kV were carried out for the microstructural analysis of oxidized powders and sintered samples.

The density of the sintered materials was measured by Archimedes method (Table 1). A slight decrease in the density of all sintered samples with the increase of oxidation time was observed. The hardness was tested by Vicker's indentation with 10 N load was applied for 10 seconds in each case. Elastic modulus and flexural strength (3- and 4-points bending strength) of sintered samples was measured by bending tests on a tensile/loading machine (INSTRON-1112). The indentation toughness was calculated from the lengths of radial cracks and indents diagonals using a formula valid for semi-circular crack systems as proposed by Shetty [25]:

$$K_{IC} = 0.0899\ (\frac{HP}{4l})^{0.5} \quad \text{---------- (1),}$$

where H is the hardness, P is the indentation load and $l = c - a$ is the length of the indentation crack. The fractured surfaces of sintered materials were analysed by SEM.

3. Results and Discussions

3.1. Microstructural characterization

The phase analysis of base powders confirm the presence of <alpha> Si_3N_4 phase before and after the oxidation (Fig. 1). The XRD spectra of un-oxidized (reference) and oxidized Si_3N_4 powders are given in Fig. 1 and correspond mainly to <alpha> Si_3N_4 according to the JCPDS PDF (01-076-1407). The minor amorphous concentration was seen in the range of $2\theta = 15^\circ$ - 22° (Fig. 1). The presence of amorphous phase indicates the part between $2\theta = 15^\circ$ and 22° as the formation of an amorphous SiO_2 after oxidation process on the surface of the nanosized particles of Si_3N_4. The main lines of silicon oxynitride (Si_2N_2O) were detected in this range after sintering. The calculated weight of powders increased with the oxidation time that point out the oxidation of powder´s surface. Furtherly, EDX qualitative results confirmed the presence of oxygen content in powders which were subjected oxidation and it was seen that the atomic percent of oxygen increased with the oxidation time. Five times higher oxygen was detected in the case of 20 hours oxidized base powders compared with reference powder (Fig. 2 – 3).

The microstructural investigations in accordance with the phase analysis revealed the crystalline and amorphous phases in the base powders. The crystalline and amorphous phases corresponded to the Si_3N_4 and SiO_2, respectively. This amorphous SiO_2 phase was formed in the result of reaction between Si_3N_4 and O_2 during oxidation. (2) [26 - 27].

Reaction on the surface: $Si_3N_4 + 3O_2 = 3SiO_2 + 2N_2$ ---------- (2)

The thickness of amorphous SiO_2 phase was observed 1.5 nm and 4 nm with the oxidation time of 10 hours and 20 hours, respectively (Fig. 4). The SiO_2 layer on the silicon nitride particles might act as a protective layer and slowed down the reaction between oxygen and silicon nitride. It is proposed that the thickness of layer was the controlling step of the oxidation of powder particles.

The morphology of un-oxidized and oxidized Si_3N_4 powders are shown in Fig. 4. In all cases, the base powders before and after oxidation showed the globular morphology. The observed grain size was bimodal, 50 nm and 500 nm. The amorphous oxide layer was observed on surface of oxidized grains, ~ 1.5 nm in case of 10h and ~ 4 nm in case of 20 h oxidization process (Fig. 4). Based on HRTEM investigations, the oxygen-containing crystals were not located at the Si_3N_4 grain boundaries, as shown in the Fig. 5, where the SiO_2 amorphous phase was located earlier in the base powders (Fig. 4). It was expected that the amorphous phase will be present in the sintered samples due to the presence of amorphous SiO_2 phase on the particles of base powders. The HRTEM images of sample 1700/20 reveal that the amorphous phases are not present at the grain boundaries. The clear grain boundaries could be seen between the Si_3N_4 grains. The same results are expected in the remaining samples as 1700/20 (Fig. 5). After the sintering at 1500 and 1700 $^\circ$C under 20 MPa pressure for 3 hours, the structural peaks of <alpha> phase and <beta> phase of Si_3N_4, silicon oxynitride (Si_2N_2O) and ZrO_2 phases were detected (Fig. 6). ZrO_2 is assumed to be the contamination which was originated from the milling media (ZrO_2 balls). The <alpha> Si_3N_4 JCPDS PDF (01-076-1407), <beta> Si_3N_4 JCPDS PDF (00-33-1160), Si_2N_2O JCPDS PDF (00-47-1627) and ZrO_2 JCPDS PDF (00-83-0944) were identified. The complete transformation of <alpha> to

<beta> phase of Si_3N_4 was found and the <alpha> grains were dissolved in a liquid phase and precipitated as <alpha> phase in the samples sintered at 1700 ˚C (1700/0, 1700/10 and 1700/20). On the other hand at 1500 ˚C (Samples: 1500/0, 1500/10 and 1500/20), the incomplete transformation was observed because the sintering temperature was lower than the transformational temperature [28 - 29]. Si_2N_2O was formed from the reaction of SiO_2 and Si_3N_4 in the presence of liquid phase [30 - 31]. The study of this work showed that the oxidized powders contained oxygen which caused the formation of Si_2N_2O in the presence of liquid phases. In the first step, the SiO_2 was formed (3) on the surface of the Si_3N_4 powder particles and in the second step, reaction was occurred between SiO_2 and Si_3N_4 in the presence of N_2 gas environment during the sintering process at higher temperatures. The increasing Si_2N_2O amount was observed with the increasing amount of oxygen content in powders which is the function of oxidation time (4) (Fig. 4).

Reaction on the surface:

$$Si_3N_4 + 3O_2 = 3SiO_2 + 2N_2 \text{ ---------- (3)}$$

Reaction during sintering process:

$$SiO_2 + Si_3N_4 = 2Si_2N_2O \text{ ---------- (4)}$$

The maximum content of <beta> Si_3N_4 was found to be ~ 78 wt.% in un-oxidized sample, sintered at 1700 ˚C (Table 1). The obtained amount of <beta> phase decreased with the oxidation time (Fig. 7) while Si_2N_2O phase increased linearly with the oxidation time (Fig. 8a). It is consistent with study of Park et al. [32]. They showed that <beta> phase decreased with the increase of Si_2N_2O. In the case of sintered samples at 1700 ˚C, Si_2N_2O phase increased with same growth rate as <beta> Si_3N_4 decreased (Fig. 8b). The amounts of Si_2N_2O and <beta> Si_3N_4 phases could be optimized with the oxidation time; the graph (Fig. 8b) shows Si_2N_2O increases and <beta> Si_3N_4 decreases equally with respect to oxidation time. The growth rate of Si_2N_2O phase in the samples sintered at 1500 ˚C was slightly higher than the transformation rate of <alpha> to <beta> phase of Si_3N_4 (Fig. 8c). It is assumed that the temperature of formation of Si_2N_2O was lower than the temperature of <alpha> to <beta> transformation because almost similar amount of Si_2N_2O was observed at 1500 ˚C and 1700 ˚C. The 23 wt. % and 25 wt. % of Si_2N_2O was detected in the sintered samples at 1500 ˚C and 1700 ˚C respectively but <beta> concentration was different at both temperatures; this was ~~is~~ the indication that Si_2N_2O was formed at lower temperature than the <alpha> to <beta> transformational temperature. The crystallite size of <beta> phase in all samples decreased with the increase in oxidation time but the crystallite size of Si_2N_2O increased with the increase in oxidation time. The formation of Si_2N_2O started at lower temperature than the <alpha> to <beta> transformation temperature and the higher concentration of oxygen in base powders favoured the formation of Si_2N_2O and hindered the crystallite growth of <beta> phase of Si_3N_4.

The morphological study of fractured surfaces of 1500/0, 1500/10 and 1500/20 revealed the presence of internal porosity and more likely, the fractures are initiated from these porous points (Fig. 14). Unlike the samples sintered at 1500 ˚C, the porosity in samples sintered at 1700 ˚C could not be observed by microstructural examination (Fig. 15). The rod-like <beta> grains and bright Si_2N_2O phases are visible. The crack growth was inter-granular and trans-granular in the samples. It could be seen a few fractures happened in hexagonal <beta> grains but mainly went along the grain boundaries (trans-granular) and Si_2N_2O grains.

3.2. Mechanical Properties

The <alpha>/<beta> ratio and Si_2N_2O phases influence the mechanical properties. The 4-point bending strength of samples sintered at 1500 ˚C were in the range of 300 ÷ 320 MPa (Fig. 9). This value decreased slightly with the increase of oxidation time. The 4- point bending strength of samples sintered at 1700 ˚C is two times higher in the range of 600 ÷ 775 MPa (Fig. 9). Un-oxidized sample (1700/0) with highest 78% of <beta> Si_3N_4 phase showed the highest value and followed by 1700/10 and 1700/20. The flexural strength decreased due to the decrease in the amount of <beta> phase with the increase in oxidation time. The <beta> phase are rod-like elongated hexagonal grains which act as reinforcing agent in the matrix and strengthen the composite. The decrease in strength can be seen with the increase in oxidation time in Fig. 9. The degradation in strength is due to the decrease in amount of <alpha> Si_3N_4 and increase in amount of Si_2N_2O phases in the sample with the oxidation time. The <beta> Si_3N_4 to Si_2N_2O ratio is important for optimizing the flexural strength. The presence of internal porosity was revealed by the morphological study of fractured surfaces of all samples sintered at 1500 ˚C (Fig. 14) and the porosity contributed in decreasing the flexural strength. The fracture was nucleated from the porous sites and propagated through inter-granular and trans-granular sites. The 4- point bending strength of samples sintered at 1500 ˚C are much lower than that of samples sintered at 1700 ˚C. The lower flexural strength in case of samples sintered at 1500 ˚C is due to the incomplete transformation of <alpha> to <beta> phase of Si_3N_4 and internal porosity in the composite. The similar tendency for 3- point bending strength was observed in all sintered samples (Fig. 10). All samples sintered at lower temperature showed lower strength ~~values~~ than the samples sintered at higher temperature (Fig. 9 – 10). The reason of this lower strength is incomplete transformation of <alpha> to <beta> phase at 1500 ˚C. This is also fact which can be seen clearly that strength decreased with an increase in ~~of~~ silicon oxynitride (Si_2N_2O). The <beta> Si_3N_4 phase decreased with the increase in ~~of~~ oxidation time, which lowered the strength of the samples. The strength of 1700/0 (reference) is higher because it has the highest content of <beta> phase. The elastic modulus (E) identifies the stiffness and depends on porosity, grain boundary phases, texture and relative contents of α and β phases was measured in the range between 240 and 260 GPa (Fig. 11). In the case of sintering temperature 1500 ˚C, the value is constant and no effect of oxidation time on the elastic modulus was observed compared to samples sintered at 1700°C. The elastic modulus of 1700/0, 1700/10 and 1700/20 decreased with the increasing of the oxidation time. The same decreasing trend was observed for bending strength of these samples. These differences can be explained by some parameters; the sintering temperature

and the oxidation time, the <alpha>/<beta> phase ratio, <beta>Si_3N_4/Si_2N_2O and the differences in the apparent density of the samples. The samples with higher densities showed higher values, respectively. The toughness (K_{IC}) values of all the samples sintered at 1500 ˚C are in the range of 10 ÷ 11 MPa·$m^{1/2}$ (Fig. 12). The sample 1500/20 has the highest toughness among the samples which were sintered at 1500 ˚C. More likely the reason is sample 1500/20 contains the ~~a~~ higher content of <beta> phase among the samples of this series. The toughness values of all the samples sintered at 1700 ˚C were in the range of 8 ÷ 13 MPa·$m^{1/2}$. The highest toughness was observed in the sample 1700/0 which is 13 MPa·$m^{1/2}$. The toughness decreased with the decrease of <beta> phases and the oxidation time. Park et. al. [32] reported the higher toughness with the higher amount of Si_2N_2O in the sample but this study disagreed with this fact and reported the decrease in ~~of~~ toughness with the increase of Si_2N_2O. The Vicker's hardness values of samples sintered at 1500 ˚C are higher compared to the samples sintered at 1700 ˚C (Fig. 13). The positive effect of oxidation time can be observed to some extent in the hardness values of samples 1500/0, 1500/10 and 1500/20. The highest hardness value was observed in the case of 10 hours oxidation sample (1500/10) and the hardness started decreasing after 10 hours oxidation. In the case of samples sintered at 1700 ˚C (1700/0, 1700/10 and 1700/20), a different trend of hardness was observed. The hardness of 10 hours oxidized sample has the highest hardness and lowest hardness in 20 hours oxidized sample case. The un-oxidized sample has the hardness value in between the values of 10 hours and 20 hours oxidized samples. The samples 1500/0, 1500/10 and 1500/20 contain a higher amount of <alpha> Si_3N_4 than that of samples 1700/0, 1700/10 and 1700/20. The <alpha> phase of Si_3N_4 is harder than the <beta> Si_3N_4. The higher content of <alpha> phase in 1500/0, 1500/10 and 1500/20 contributes in the hardening of the material and the higher values of hardness were observed in these samples. It was also observed that the oxidation time has a positive effect on the hardness of both series of samples to some extent.

4. Conclusions

The effect of nanosized oxidized silicon powder particles on the microstructural and mechanical properties of hot isostatic pressed silicon nitride was studied.

- <alpha> Si_3N_4 powders were oxidized for 10 and 20 hours successfully and the amorphous oxide layer was found on the Si_3N_4 particles.
- The complete <alpha> to <beta> phase transformation was observed at 1700 ˚C under 20 MPa for 3 hours holding time, 1500 ˚C is insufficient sintering temperature for the complete phase transformation.
- Si_2N_2O phase was formed in the samples after sintering and this amount increased with the oxidation time.
- There is a threshold of powder oxygen content (2.29 at% given by EDS) above that the Si_2N_2O phase is stabilized even at higher temperatures. Oxides in the base

powders favours the formation of Si_2N_2O and supress the <beta> Si_3N_4 in sintered material.

- The bending strength of those samples which were prepared at 1700 ˚C is higher than that of samples sintered at 1500 ˚C due to the presence of <beta> phase and Young's modulus is almost similar of both set of samples. The optimum sintering temperature is 1700 ˚C when the bending strength decreased with the oxidation time.
- The toughness decreased with the oxidation time due to the decreasing amount of <beta> Si_3N_4.
- Higher hardness was observed in the samples which contain higher <alpha> Si_3N_4.

In conclusion, the oxidation of starting powders degrades the mechanical properties of hot isostatic pressed (HIP) Si_3N_4.

Acknowledgement

Awais Qadir thanks for the Stipendium Hungaricum Scholarship Program. We acknowledge the support given by the Hungarian National Research Development and Innovation Office for the funding of M-ERA.NET Project "Graphene-ceramic composites for tribological application in aqueous environments" and FLAG-ERA "Multifunctional Ceramic/Graphene Coatings for New Emerging Applications". Thanks to Mr. V. Varga for sample preparation, Mr. L. Illés from MTA EK performing SEM measurements.

Reference

[1] S. Hampshire, Silicon nitride ceramics - review of structure, processing and properties, J. Achiev. Mater. Manuf. Eng. 24 (1) (2007) 43–50.
[2] H. Klemm, Silicon Nitride for High-Temperature Applications, J. Am. Ceram. Soc. 93(6)(2010)1501–1522.
[3] T.F. Ariff, N.S. Shafie, and Z.M. Zahir, Wear Analysis of Silicon Nitride (Si_3N_4) Cutting Tool in Dry Machining of T6061 Aluminium Alloy, Appl. Mech. Mater. 268–270 (2013) 563–567.
[4] G. Petzow and M. Herrmann, Silicon Nitride Ceramics, in High Performance Non-Oxide Ceramics II, Structure and Bonding, Publ. Springer-Verlag Berlin Heidelberg, 2002, pp. 47
[5] E. Gugel and G. Woetting, Materials selection for ceramic components in automobiles, in Advances in science and technology, (1999), pp. D285–D296.
[6] G. Wötting, J. Hennicke, K.H. Feuer H, Thiemann, D. Vollmer, E. Fechter, F. Sticher, A. Geyer, Reliability and Reproducibility of Silicon Nitride Valves: Experiences of a Field Test," in Ceramic Materials and Components for Engines, J. G. Heinrich and F. Aldinger, Eds. Wiley-VCH Verlag GmbH, 2001, pp. 181–185.
[7] D. Hardie and K.H. Jack, Crystal Structures of Silicon Nitride, Nature 180 (4581) (1957) 332–333.
[8] A. Zerr, G. Miehe, G. Serghiou, M. Schwarz, E. Kroke, R. Riedel, H. Fueß, P. Kroll, R. Boehler, Synthesis of cubic silicon nitride, Nature 400(6742) (1999) 340–342.

[9] H. Suematsu, M. Mitomo, T. E. Mitchell, J. J. Petrovic, O. Fukunaga, and N. Ohashi, The α–β Transformation in Silicon Nitride Single Crystals, J. Am. Ceram. Soc. 80(3) (1997) 615–620.
[10] L.J. Bowen, R.J. Weston, T.G. Carruthers, R.J. Brook, Hot-pressing and the α-β phase transformation in silicon nitride, J. Mater. Sci. 13(2) (1978) 341–350.
[11] P. F. Becher, Microstructural Design of Toughened Ceramics, J. Am. Ceram. Soc. 74(2) (1991) 255–269.
[12] X. Zhu and Y. Sakka, Textured silicon nitride: processing and anisotropic properties, Sci. Technol. Adv. Mater. 9(3) (2008) 033001.
[13] J. Gubicza, P. Arató, F. Wéber, A. Juhász, Mechanical properties of oxidized silicon nitride ceramics, Mater. Sci. Eng. A 259(1) (1999) 65–72.
[14] C. He, L. Wang, J. Wu, Oxidation of sintered silicon nitride, J. Mater. Sci. 28(18) (1993) 4829–4834.
[15] H.-J. Choi, Y.-W. Kim, J.-G. Lee, High temperature strength and oxidation behaviour of $Er_2Si_2O_7$-Si_3N_4 ceramics, J. Mater. Sci. Lett. 15(4) (1996) 282–284.
[16] Y. Ukyo, The effect of a small amount of impurity on the oxidation of Si_3N_4 ceramics, J. Mater. Sci. 32(20) (1997) 5483–5489.
[17] M. K. Cinibulk and H.-J. Kleebe, Effects of oxidation on intergranular phases in silicon nitride ceramics, J. Mater. Sci. 28(21) (1993) 5775–5782.
[18] A. Rendtel, G. Grathwohl, F. Tümmler, Oxidationsbedingte Veränderungen der Phasenzusammensetzung von dichten Siliciumnitrid (SSN), CFI Ceram. Forum Int. 69(5-6) (1992) 199–204.
[19] C. Balázsi, F.S. Cinar, O. Addemir, F. Wéber, P. Arató, Manufacture and examination of C/Si_3N_4 nanocomposites, J. Eur. Ceram. Soc. 24(12) (2004) 3287–3294.
[20] K. Okada, K. Fukuyama, Y. Kameshima, Characterization of Surface-Oxidized Phase in Silicon Nitride and Silicon Oxynitride Powders by X-ray Photoelectron Spectroscopy, J. Am. Ceram. Soc 78(8) (1995) 2021–2026.
[21] S. Natansohn, A. E. Pasto, and W. J. Rourke, Effect of Powder Surface Modifications on the Properties of Silicon Nitride Ceramics, J. Am. Ceram. Soc. 76(9) (1993) 2273–2284.
[22] P.S. Wang, S.G. Malghan, S.M. Hsu, and T.N. Wittberg, Effects of α-silicon nitride powder processing on surface oxidation kinetics, J. Mater. Res. 8(12) (1993) 3168–3175.
[23] J. C. Rivière, J. a. A. Crossley, B. A. Sexton, Silicon oxynitride films: Ion bombardment effects, depth profiles, and ionic polarization, studied with the aid of the Auger parameter, J. Appl. Phys. 64(9) (1988) 4585–4600.
[24] C. Balázsi, Zs. Fogarassy, O. Tapasztó, A. Kailer, Ch. Schröder, M. Parchoviansky, D. Galusek, J. Dusza, K. Balázsi, Si_3N_4/graphene nanocomposites for tribological application in aqueous environments prepared by attritor milling and hot pressing, J. Eur. Ceram. Soc. 37(12) (2017) 3797–3804
[25] D.K. Shetty, I.G. Wright, P.N. Mincer, A.H. Clauer, Indentation fracture of WC-Co cermets, J. Mater. Sci. 20(5) (1985) 1873–1882.
[26] I.S. Kainasskii, E.V. Degtyareva, V.A. Kukhtenko, Carborundum Products Bonded with Silicon Nitride, Ogneupory 25(4) (1960) 175–80.
[27] K.H. Stern, Oxidation of Silicon, Silicon Carbide (SiC) and Silicon Nitride (Si_3N_4), Publ. NAVAL RESEARCH LAB WASHINGTON DC, 1986.
[28] D. Bučevac, S. Bošković, B. Matović, Kinetics of the α-β phase transformation in seeded Si_3N_4 ceramics, Sci. Sinter. 40(3) (2008) 263–270.

[29] L. Wang, T.-Y. Tien, I.-W. Chen, Formation of β-Silicon Nitride Crystals from (Si,Al,Mg,Y)(O,N) Liquid: I, Phase, Composition, and Shape Evolutions, J. Am. Ceram. Soc. 86(9) (2003) 1578–1585.
[30] Z. K. Huang, P. Greil, G. Petzow, Formation of silicon oxinitride from Si_3N_4 and SiO_2 in the presence of Al_2O_3, Ceram. Int. 10(1) (1984) 14–17.
[31] B. Bergman and H. Heping, The influence of different oxides on the formation of Si_2N_2O from SiO_2 and Si_3N_4, J. Eur. Ceram. Soc. 6(1) (1990) 3–8.
[32] D.-S. Park, H.-J. Choi, B.-D. Han, H.-D. Kim, and D.-S. Lim, Effect of Si_2N_2O content on the microstructure, properties, and erosion of silicon nitride–Si_2N_2O in situ composites, J. Mater. Res. 17(9) (2002) 2275–2280.

Table 1

Nr.	**1500/0**	**1500/10**	**1500/20**	**1700/0**	**1700/10**	**1700/20**
Oxidation Time (hrs)	0	10	20	0	10	20
Sintering Temperature (˚C)	1500	1500	1500	1700	1700	1700
Apparent Density (g/cm^3)	3.330	3.303	3.27	3.431	3.387	3.352
$\frac{\beta - Si_3N_4}{Si_2N_2O}$	$\frac{12.8}{12.6}$, (1 : 1)	$\frac{5}{17.8}$, (0.28 : 1)	$\frac{10}{23}$, (0.434 : 1)	$\frac{78}{6.7}$, (11 : 1)	$\frac{60}{20.5}$, (2.92 : 1)	$\frac{56.4}{25.8}$, (2.18 : 1)
Average size of β-Si_3N_4 (nm)	39.39 ± 4.42	39.65 ± 4.57	37.14 ± 4.05	60.81 ± 8.38	56.75 ± 8.28	56.37 ± 8.46
Average size of Si_2N_2O (nm)	52.53 ± 4.40	55.18 ± 4.50	51.90 ± 4.01	37.72 ± 8.40	62.71 ± 8.29	64.18 ± 8.47

- calculated by **Scherer Formula**

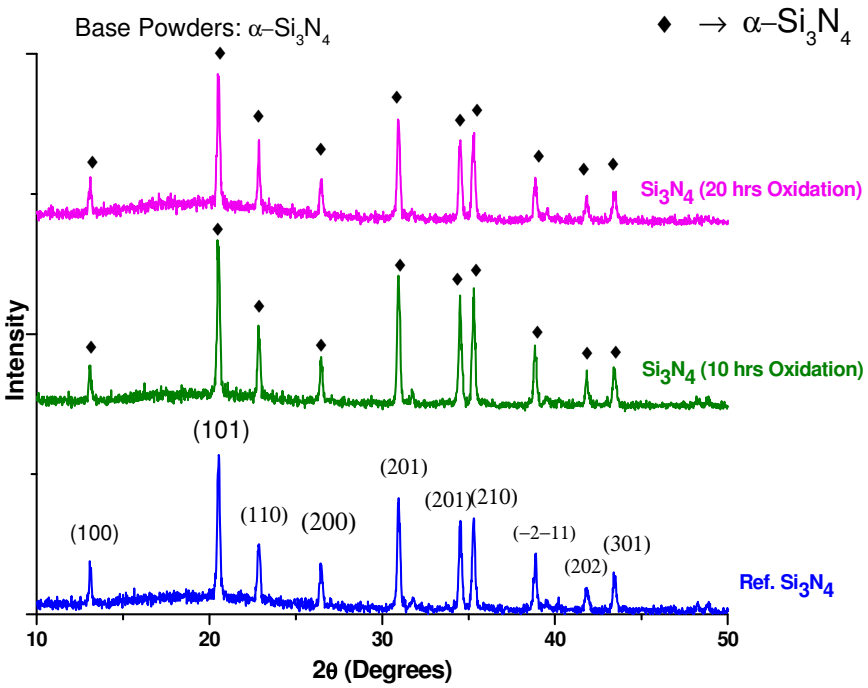
Base Powders: α–Si3N4
♦ → α–Si3N4
Si3N4 (20 hrs Oxidation)
Si3N4 (10 hrs Oxidation)
Ref. Si3N4
Intensity
(100)
(101)
(110)
(200)
(201)
(201)
(210)
(–2–11)
(202)
(301)
10
20
30
40
50
2θ (Degrees)

Fig. 1.

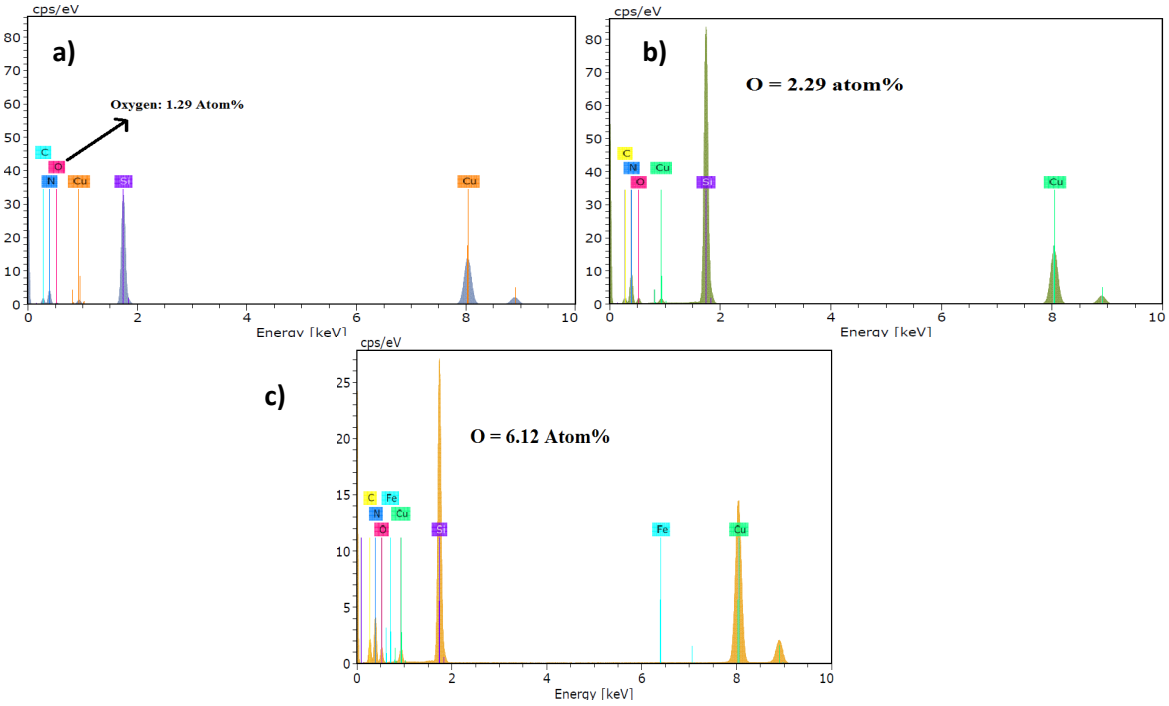
cps/eV
a)
Oxygen: 1.29 Atom%
C
O
N
Cu
Si
Cu
Energy [keV]
cps/eV
b)
O = 2.29 atom%
C
N
Cu
O
Si
Cu
Energy [keV]
c)
cps/eV
O = 6.12 Atom%
C
Fe
N
Cu
O
Si
Fe
Cu
Energy [keV]

Fig. 2.

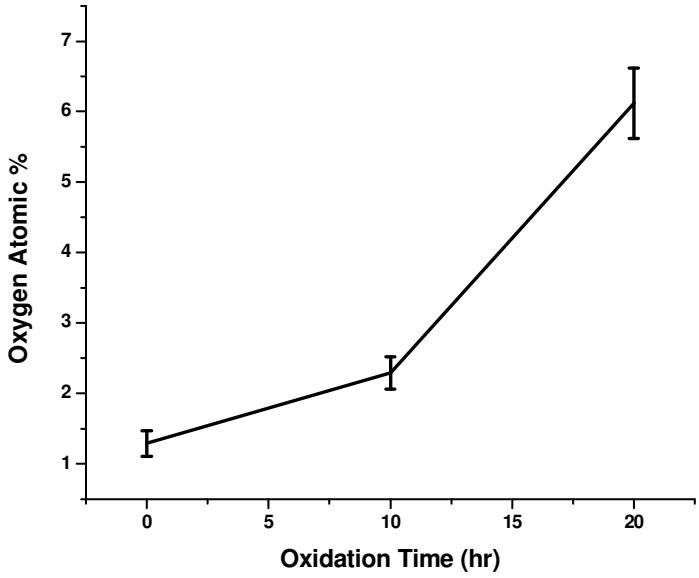
Oxygen Atomic %
Oxidation Time (hr)

Fig. 3.

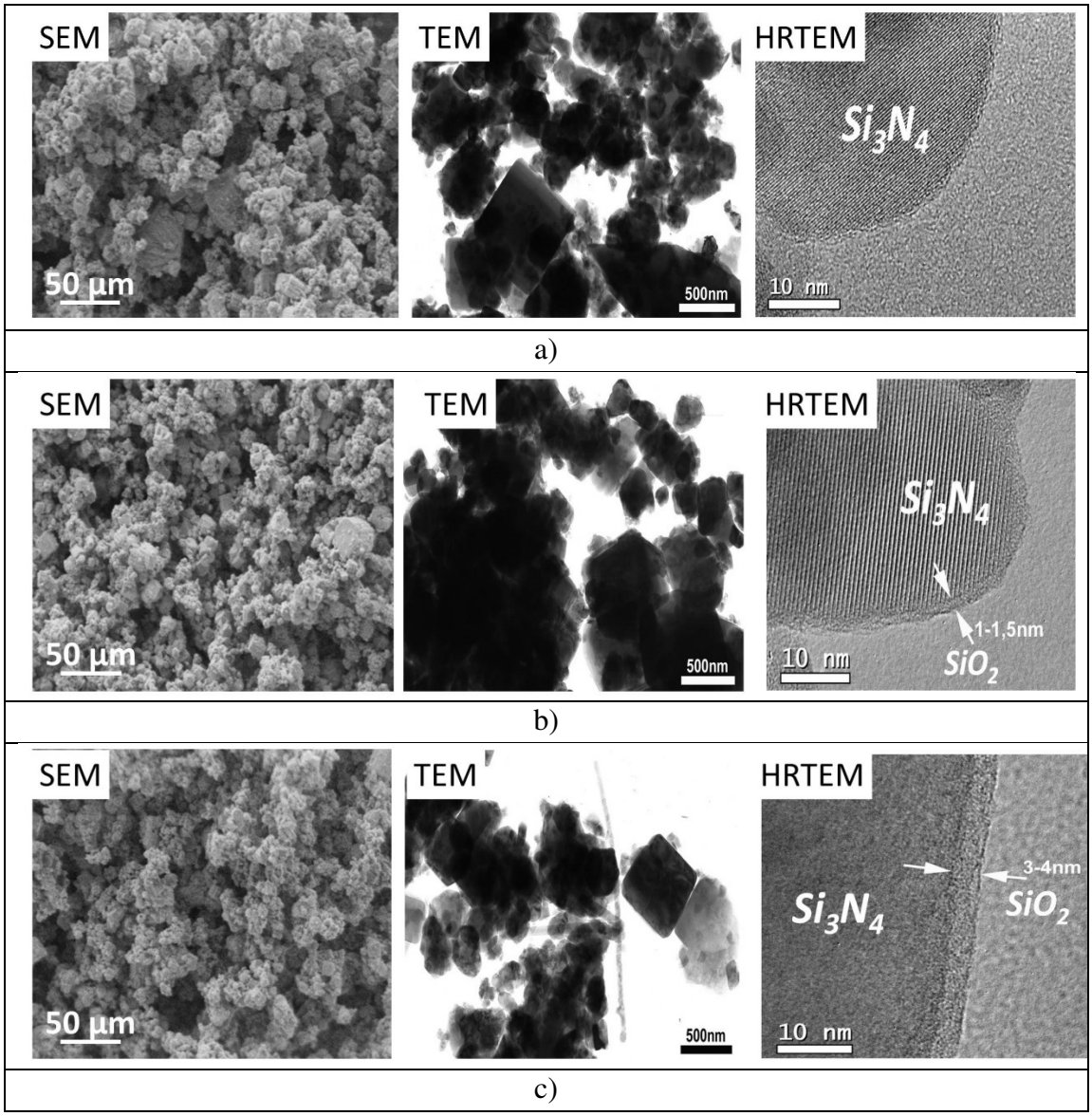
SEM
TEM
HRTEM
Si_3N_4
50 µm
500nm
10 nm
a)
SEM
TEM
HRTEM
Si_3N_4
1-1,5nm
50 µm
500nm
10 nm
SiO_2
b)
SEM
TEM
HRTEM
3-4nm
Si_3N_4
SiO_2
50 µm
500nm
10 nm
c)

Fig. 4.

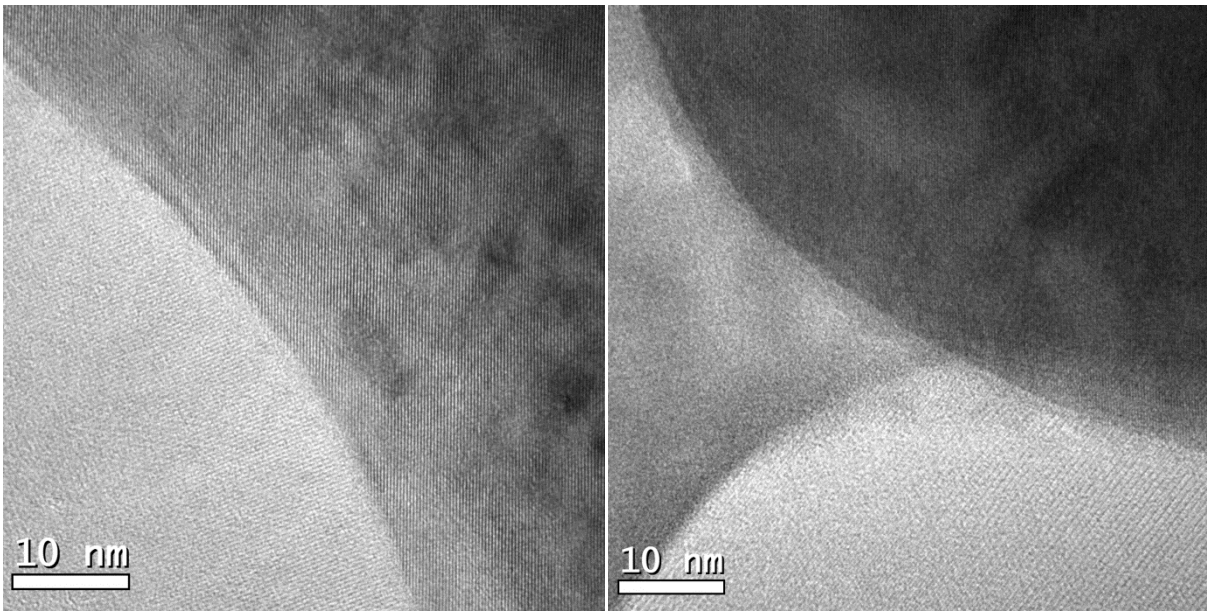

Fig. 5.

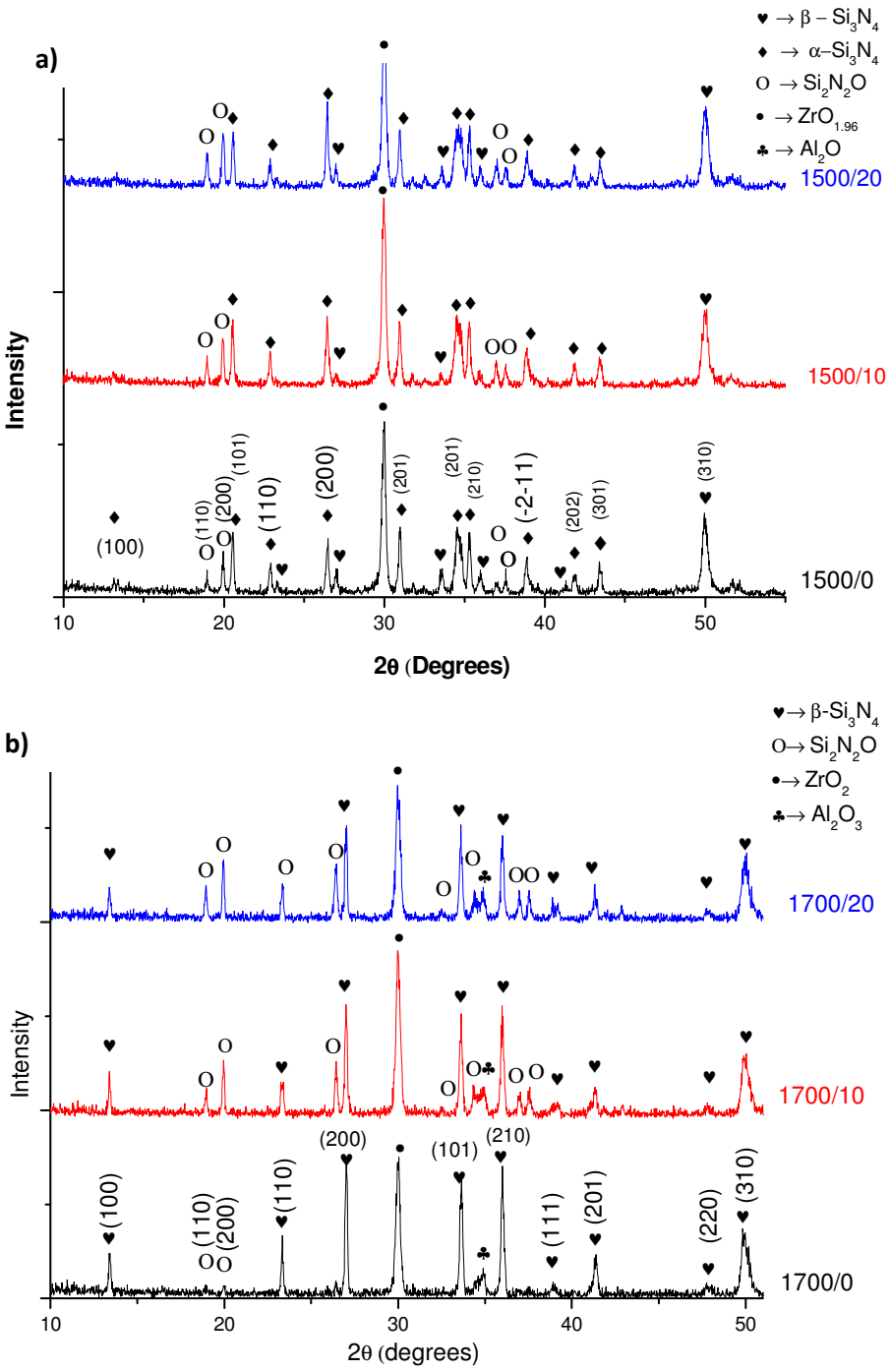
a)
♥ → β – Si3N4
♦ → α–Si3N4
O → Si2N2O
• → ZrO1.96
♣ → Al2O
1500/20
1500/10
1500/0
Intensity
(100)
(110)
(200)
(101)
(110)
(200)
(201)
(201)
(210)
(-2-11)
(202)
(301)
(310)
10
20
30
40
50
2θ (Degrees)
b)
♥→ β-Si3N4
O→ Si2N2O
•→ ZrO2
♣→ Al2O3
1700/20
1700/10
1700/0
Intensity
(100)
(110)
(200)
(110)
(200)
(101)
(210)
(111)
(201)
(220)
(310)
10
20
30
40
50
2θ (degrees)

Fig. 6.

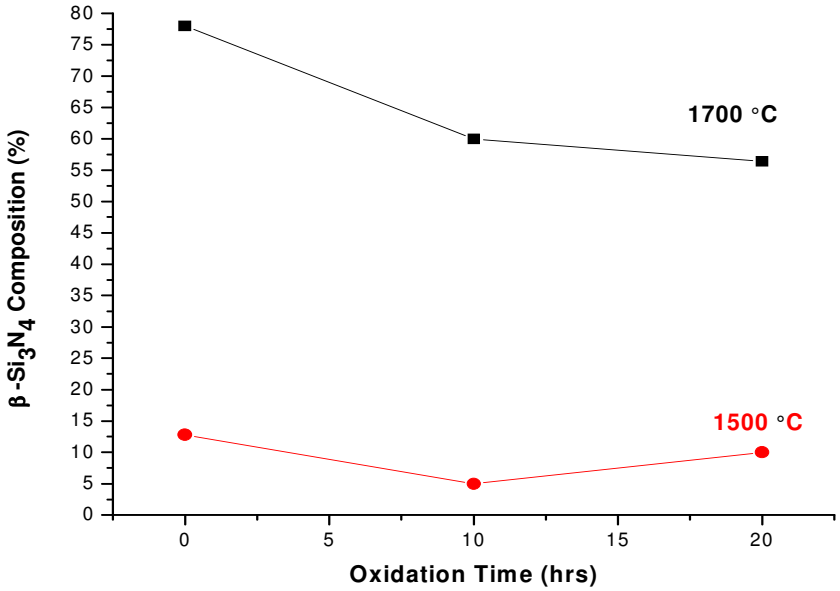
β-Si3N4 Composition (%)
Oxidation Time (hrs)
1700 °C
1500 °C
0
5
10
15
20
0
5
10
15
20
25
30
35
40
45
50
55
60
65
70
75
80

Fig. 7.

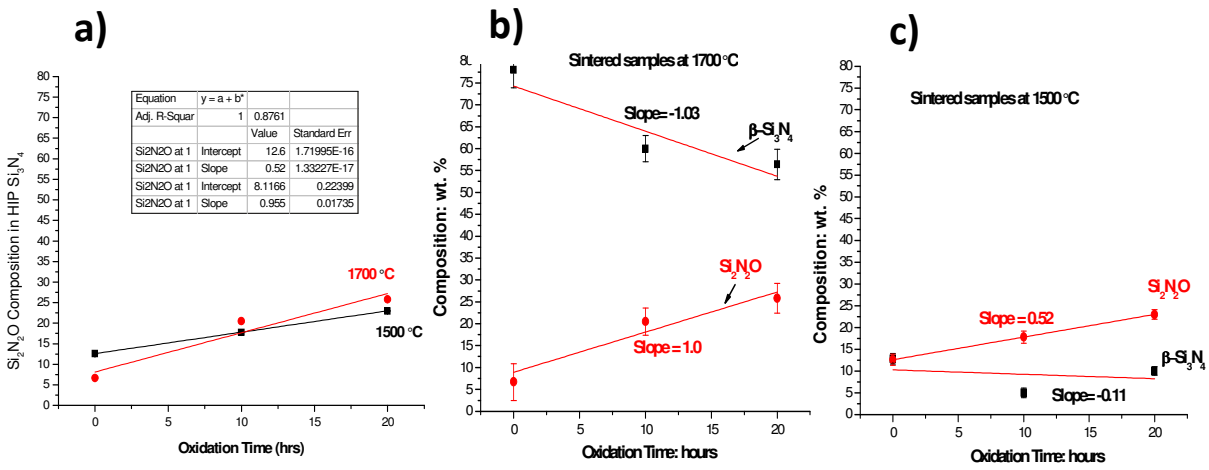
a)
b)
c)
Equation
y = a + b*
Adj. R-Squar
1
0.8761
Value
Standard Err
Si2N2O at 1
Intercept
12.6
1.71995E-16
Si2N2O at 1
Slope
0.52
1.33227E-17
Si2N2O at 1
Intercept
8.1166
0.22399
Si2N2O at 1
Slope
0.955
0.01735
1700 °C
1500 °C
Si2N2O Composition in HIP Si3N4
Oxidation Time (hrs)
Sintered samples at 1700 °C
Slope= -1.03
β-Si3N4
Si2N2O
Slope = 1.0
Composition: wt. %
Oxidation Time: hours
Sintered samples at 1500 °C
Slope = 0.52
Slope= -0.11

Fig. 8.

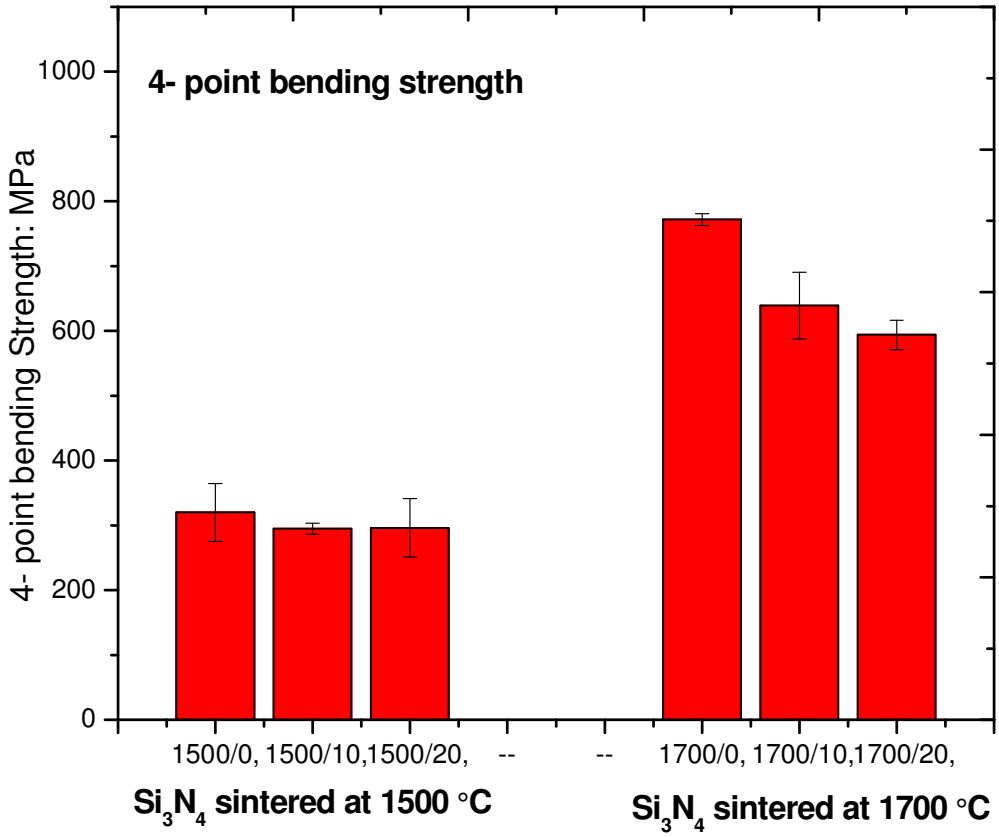
4- point bending strength
4- point bending Strength: MPa
1000
800
600
400
200
0
1500/0, 1500/10,1500/20,
--
--
1700/0, 1700/10,1700/20,
Si3N4 sintered at 1500 °C
Si3N4 sintered at 1700 °C

Fig. 9.

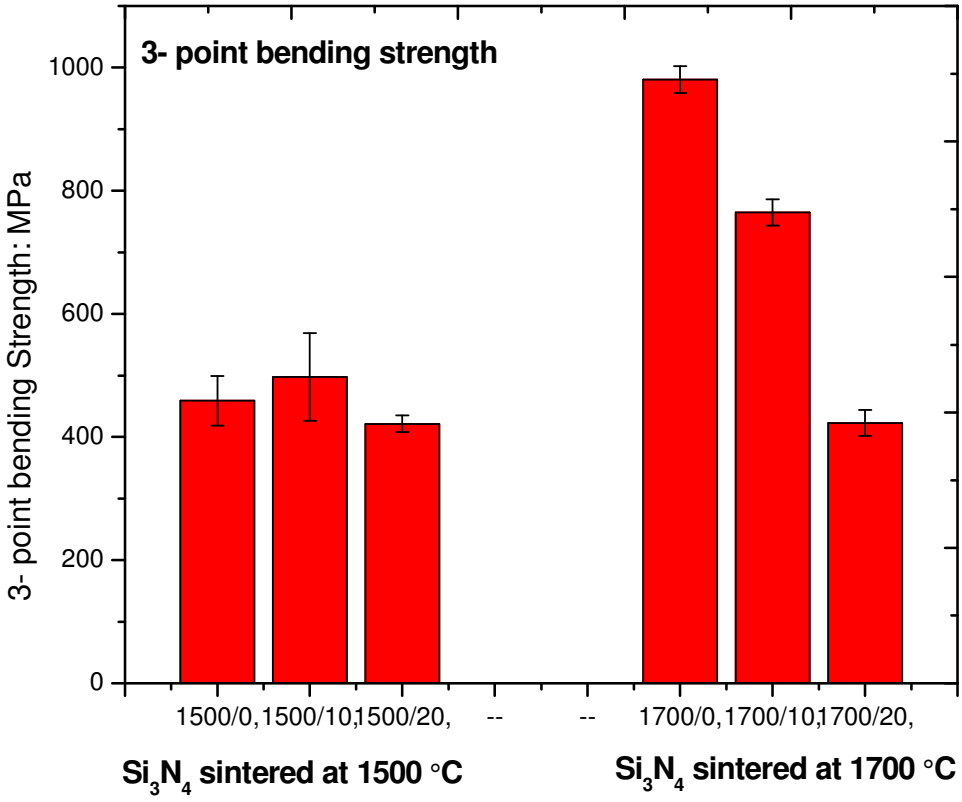
3- point bending strength
3- point bending Strength: MPa
1000
800
600
400
200
0
1500/0,1500/10,1500/20,
--
--
1700/0,1700/10,1700/20,
Si3N4 sintered at 1500 °C
Si3N4 sintered at 1700 °C

Fig. 10.

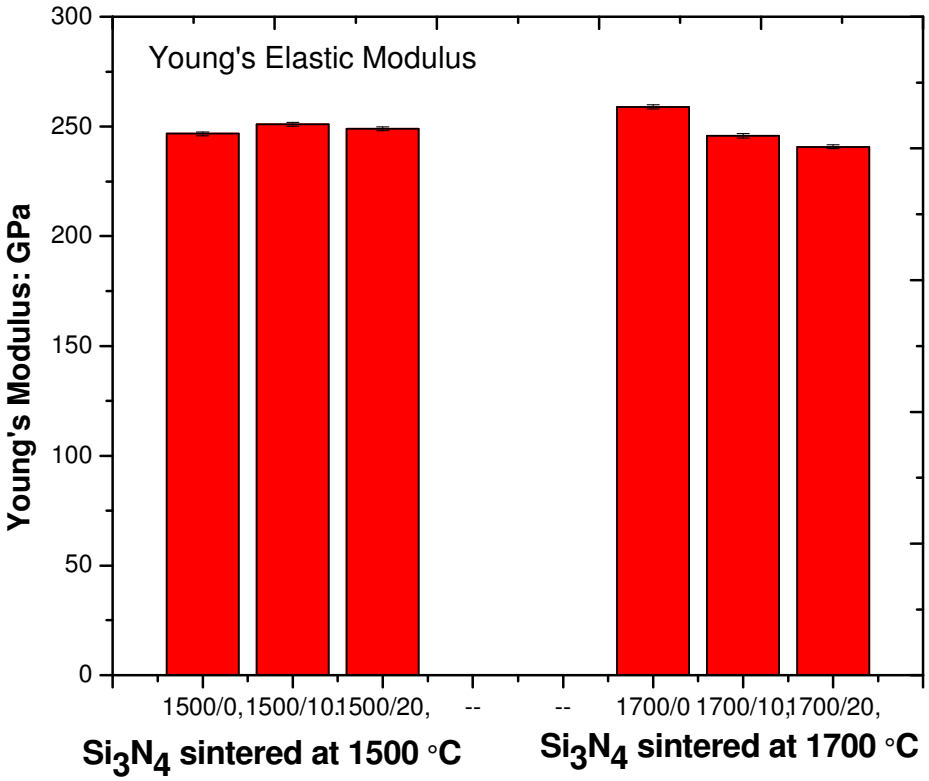
Young's Elastic Modulus
Young's Modulus: GPa
300
250
200
150
100
50
0
1500/0,
1500/10,
1500/20,
--
--
1700/0
1700/10,
1700/20,
Si3N4 sintered at 1500 °C
Si3N4 sintered at 1700 °C

Fig. 11.

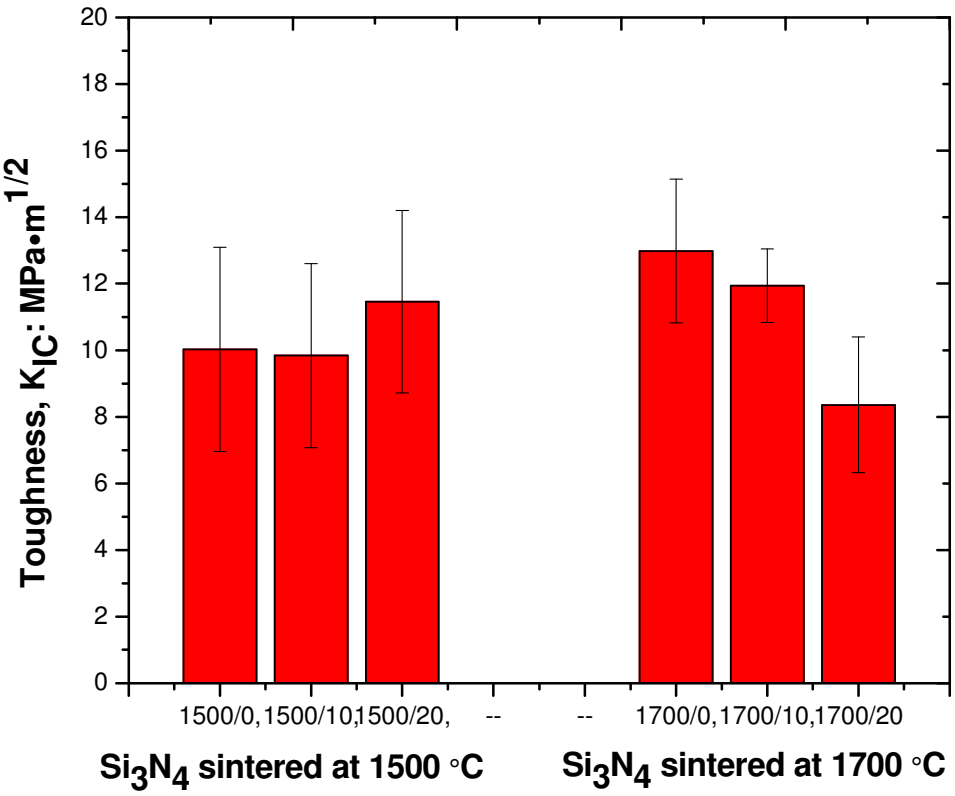
Toughness, K_{IC}: MPa•m$^{1/2}$
20
18
16
14
12
10
8
6
4
2
0
1500/0,
1500/10,
1500/20,
--
--
1700/0,
1700/10,
1700/20
Si_3N_4 sintered at 1500 °C
Si_3N_4 sintered at 1700 °C

Fig. 12.

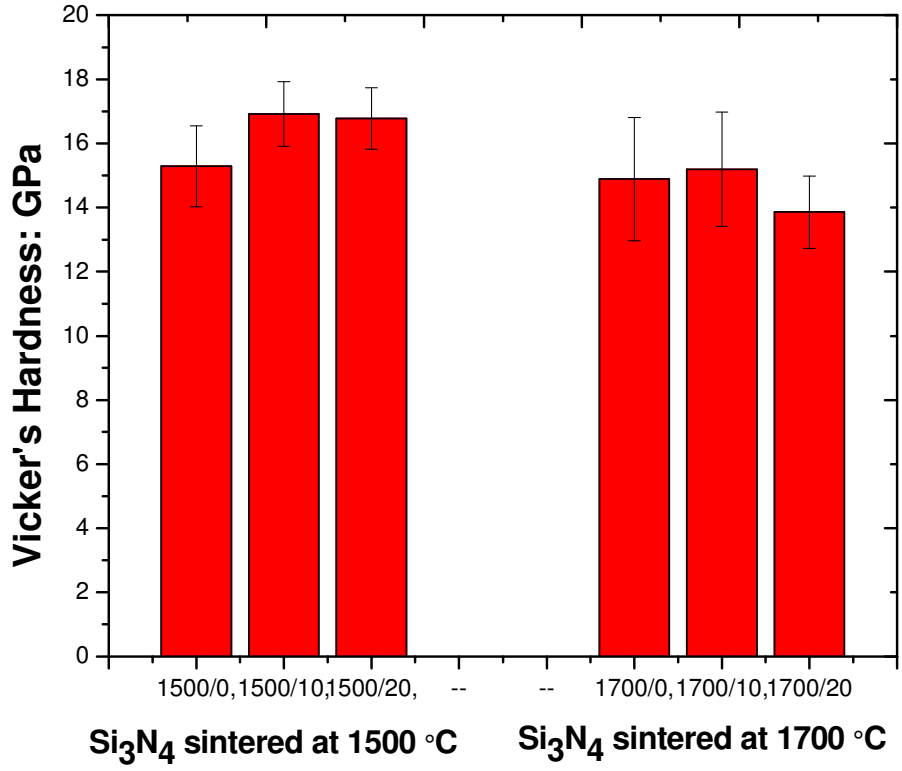
Vicker's Hardness: GPa
20
18
16
14
12
10
8
6
4
2
0
1500/0,1500/10,1500/20,
--
--
1700/0,1700/10,1700/20
Si3N4 sintered at 1500 °C
Si3N4 sintered at 1700 °C

Fig. 13.

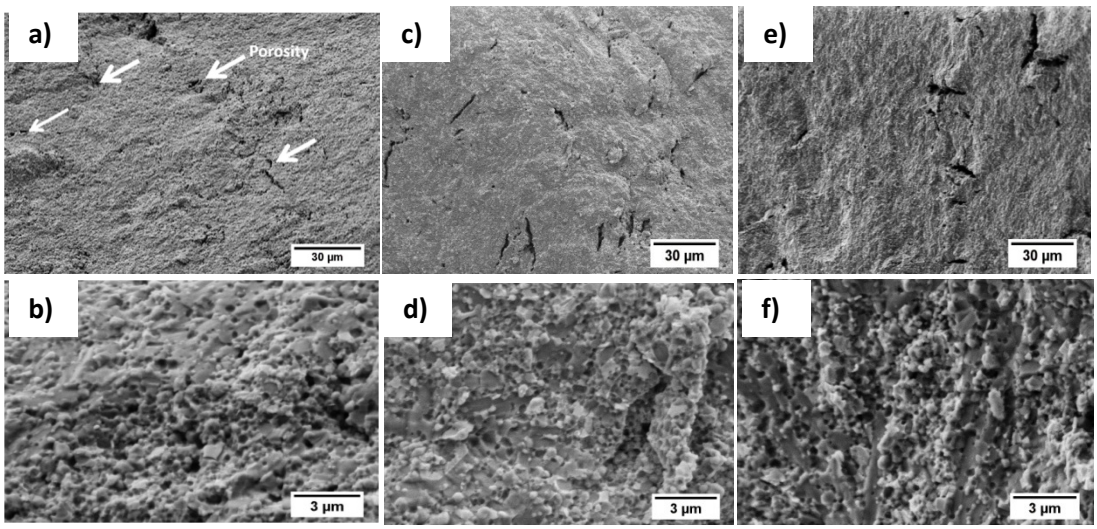

Fig. 14.

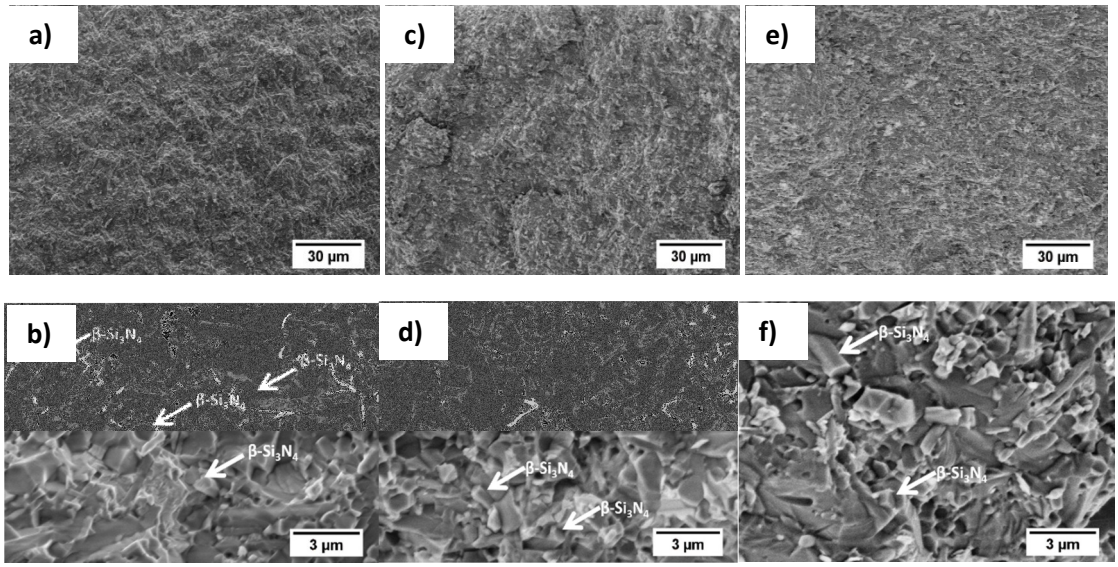

Fig. 15.

Figure Captions:

Fig. 1. XRD spectra of Reference, 10 and 20 hours oxidized Si_3N_4 base powders.

Fig. 2. EDX results of Si_3N_4 powders a) Reference; b) 10 hrs oxidized; c) 20 hrs oxidized.

Fig. 3. Oxygen content vs oxidation time of Si_3N_4 powders

Fig. 4. SEM, TEM and HREM images of Si_3N_4 base powders a) Reference; b) 10 hrs oxidized; c) 20 hrs oxidized

Fig. 5. HRTEM images of 1700/20 sample sintered at 1700 ˚C.

Fig. 6. Phase analysis of sintered Si_3N_4 samples measured by XRD. a) 1500 ˚C; b) 1700 ˚C.

Fig. 7. β phase composition in Si_3N_4 with respect to oxidation time (hrs).

Fig. 8. Si_2N_2O and β-Si_3N_4 phase in sintered Si_3N_4 with respect to oxidation time (hrs); a) Si_2N_2O in Si_3N_4; b) β-Si_3N_4 and Si_2N_2O w.r.t oxidation time in sintered samples at 1700 ˚C; c) β-Si_3N_4 and Si_2N_2O w.r.t oxidation time in sintered samples at 1500 ˚C.

Fig. 9. 4- points bending strength of Si_3N_4 samples sintered at 1500 ˚C and 1700 ˚C.

Fig. 10. 3- points bending strength of Si_3N_4 samples sintered at 1500 ˚C and 1700 ˚C.

Fig. 11. Young's Modulus measurements of Si_3N_4 samples sintered at 1500 ˚C and 1700 ˚C.

Fig. 12. Indentation toughness values of sintered materials.

Fig. 13. Vicker's Hardness of Sintered Materials

Fig. 14. SEM images of fractured surfaces of Si_3N_4 Sintered at 1500 ˚C; a & b) 1500/0 (Reference); c & d) 1500/10 (10 hrs oxidized); e & f) 1500/20 (20 hrs oxidized).

Fig. 15. SEM images of fractured surfaces Si_3N_4 (Sintered at 1700 ˚C); a & b) 1700/0 (Reference); c & d) 1700/10 (10 hrs oxidized); e & f) 1700/20 (20 hrs oxidized).